Controlling the Exciton Fine Structure Splitting in CdSe/CdS Dot-in-Rod Nanojunctions

Gabriele Rainò,[†,*] Thilo Stöferle,[†] Iwan Moreels,[†,‡,⊥] Raquel Gomes,[‡,§] Zeger Hens,[‡,§,*] and Rainer F. Mahrt[†,*]

[†]IBM Research—Zurich, Säumerstrasse 4, 8803 Rüschlikon, Switzerland, [‡]Physics and Chemistry of Nanostructures, Ghent University, Krijgslaan 281-S3, B-9000 Gent, Belgium, and [§]Center for Nano and Biophotonics, Ghent University, Belgium. [⊥]Present address: Istituto Italiano di Tecnologia, Via Morego 30, IT-16163 Genova, Italy.

ABSTRACT

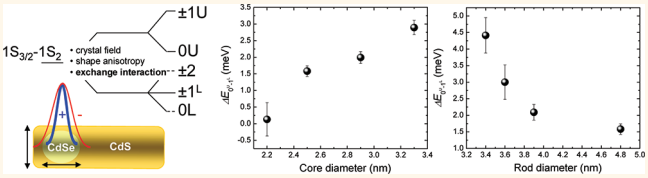

We demonstrate control and tunability of the exciton fine-structure splitting by properly engineering a nanojunction consisting of a CdSe nanocrystal core and an asymmetric rod-like CdS shell. Samples with small core and/or thick rod diameters exhibit a strongly reduced fine-structure splitting resulting from a reduced electron—hole exchange interaction. These results shed light onto the electronic configuration of such nanosystems and, apart from being of fundamental interest, could enable the use of colloidal nanocrystals as a source of entangled photons.

KEYWORDS: colloidal nanocrystals · ultrafast spectroscopy · exciton fine-structure splitting

Colloidal nanocrystals have proven to be a very versatile class of quantum nanoemitters for many different fields of applications. So far, the strong quantum confinement has mainly been used to tune the emission across the entire visible to the infrared spectral region. Besides being a unique platform to study fundamental quantum effects, these materials attract considerable interest because of their potential in optoelectronics, photonics, and the emerging field of optical quantum communication. Indeed, they have been already demonstrated to be an excellent material system for lasing and photovoltaic devices as well as a room-temperature-triggered single-photon source with high efficiency.[1−6] However, the strong confinement of the charge carriers also increases the electron—hole exchange interaction, resulting in a complicated exciton band-edge fine structure.[7] Indeed, exchange energies, *e.g.*, in CdSe, change from a few hundreds of μeV in the bulk material to tens of meV in strongly confined nanoparticles.[7−11] This is a major challenge for the realization of more advanced functionalities such as entangled photon sources. In self-assembled quantum dots (grown by molecular beam epitaxy), the biexcitonic cascade recombination with an excitonic intermediate state is used to generate polarization entangled photons. A prerequisite for the entanglement is good control of the fine-structure splitting of the bright exciton.[12−17] Therefore, in order to explore the potential for generating entangled photon pairs based on similar schemes in colloidal quantum dots, the understanding and the control of the fine-structure splitting are pivotal. Furthermore, easy processing and high room-temperature quantum efficiency make colloidal quantum dots an extremely attractive material system.

The size dependence of the fine-structure energy splitting in II—VI nanocrystals has been investigated extensively.[7−11] The general understanding is based on theoretical calculations made by Efros *et al.* using the effective mass approximation.[7] Experimental work by means of low-temperature time-resolved spectroscopy demonstrated that the emission is dominated by two states (called dark and bright state) with a relative energy splitting in reasonable agreement with that expected from theory.[8−11] More precisely, theory predicts the 8-fold degenerate exciton state to be split into five states with different energies and different projections of the angular momentum. In contrast to self-assembled quantum dots, these states are strongly coupled owing to an efficient intraband and spin relaxation

* Address correspondence to gra@zurich.ibm.com; zeger.hens@ugent.be; rfm@zurich.ibm.com.

Received for review July 26, 2011 and accepted February 24, 2012.

Published online February 24, 2012
10.1021/nn204447e

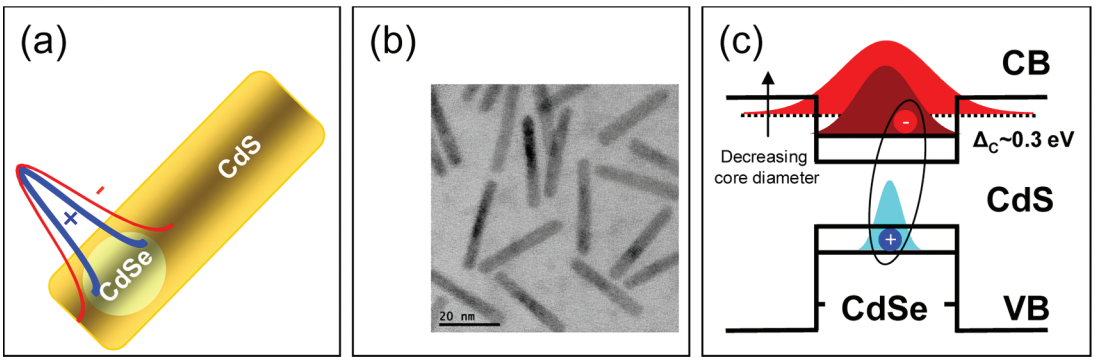

Figure 1. (a) Illustration of the CdSe/CdS dot-in-rod structure together with the expected electron–hole spatial wave function distribution. (b) Typical TEM image revealing the narrow distribution in rod diameters and lengths. (c) Band alignment for the CdSe/CdS nanojunction. Because of the small conduction-band (CB) offset ($\Delta_C \approx 0.3$ eV), tailoring the electron–hole wave function overlap is possible by properly tuning the nanojunction parameters. As an example, the sketch depicts the expected change in electron wave function distribution upon changing the core diameter. The hole energy levels and the spatial distribution of the hole wave function are affected less and remain confined in the core region because of the higher valence-band (VB) offset and the larger effective mass of the holes.

(large spin–orbit interaction by the Dresselhaus effect).[17,18]

Improvements in chemical synthesis of these nanocrystals allow control of the material composition on the subnanometer scale (up to one monolayer) and, therefore, pave the way toward the realization of high-quality nano-heterojunctions. Especially CdSe/CdS dot-in-rod structures attracted considerable attention, as they offer new prospects for tailoring the optical properties because of their small conduction-band offset.[19–22] This enables the tuning of the electron delocalization from a type I toward a quasi type II regime.[23] Moreover, a wealth of interesting physical properties have already been observed, such as an exceptional size-dependent quantum-confined Stark effect,[24] suppression of single-dot photoluminescence blinking,[5,25–27] and suppression of the Auger recombination rate, which is a prerequisite for a very long gain lifetime.[28–30] Only very recently did experiments with spherical core/giant-shell quantum dots yield first evidence of the possibility to tune the fine-structure splitting,[31] opening up new scenarios in the field of colloidal nanocrystals.

In the present work, we use precisely engineered colloidal CdSe/CdS dot-in-rod heteronanostructures to experimentally demonstrate control of the exciton fine-structure splitting by electron–hole wave function manipulation. We focus our investigation on higher lying energy states not previously explored in CdSe/CdS systems. Our results demonstrate that the fine-structure splitting can be controlled by varying the core and/or the rod diameter forming the nano-heterojunction. In particular, samples having a small core diameter and/or a thick rod diameter exhibit a strongly reduced energy splitting because of a reduced electron–hole exchange interaction. Therefore, our work expands on and extends previous work on the ability to tailor the band-edge exciton fine structure, showing a way to potentially control all electronic energy levels. Note that the dot-in-rod geometry in general adds an additional degree of freedom by allowing to engineer the shape anisotropy of the charge carrier wave functions. In addition, the already observed giant Stark effect[24] could be used for further tuning the fine-structure splitting,[16] making the dot-in-rod configuration even more appealing for practical device operation.

RESULTS AND DISCUSSION

Figure 1a provides a sketch of the samples investigated. CdSe/CdS dot-in-rods were synthesized according to an established procedure.[20] Figure 1b shows a typical transmission electron microscopy (TEM) image, illustrating the narrow dispersion in rod diameter and length. By changing the synthetic conditions, we varied the core diameter from 2.2 to 3.3 nm, whereas the rod diameter was independently tuned from 3.4 to 4.8 nm (see Supporting Information for a statistical analysis of the sizes of all samples used in this study). The band alignment is sketched in Figure 1c. As mentioned above, the small conduction band offset ($\Delta_C \approx 0.3$ eV) allows the electron–hole wave function overlap to be engineered by properly tailoring the core and rod diameter. This strongly affects the optical properties of these nanostructures, as demonstrated in Figure 2. The absorption and photoluminescence (PL) spectra of a series of samples in which either the core diameter (with the rod diameter being roughly the same) or the rod diameter (with the core being the same) has been independently changed, are reported in Figure 2a and b. Moreover, Figure 2c shows the energy difference between the first exciton absorption peaks of core-only and core–shell structures as a function of the core diameter (black markers). A larger spectral red shift is observed for structures having smaller cores. Similarly, the energy difference between the exciton absorption peaks of core-only and core–shell structures as a function of the rod diameter is shown (red markers). In this case, a larger red shift has

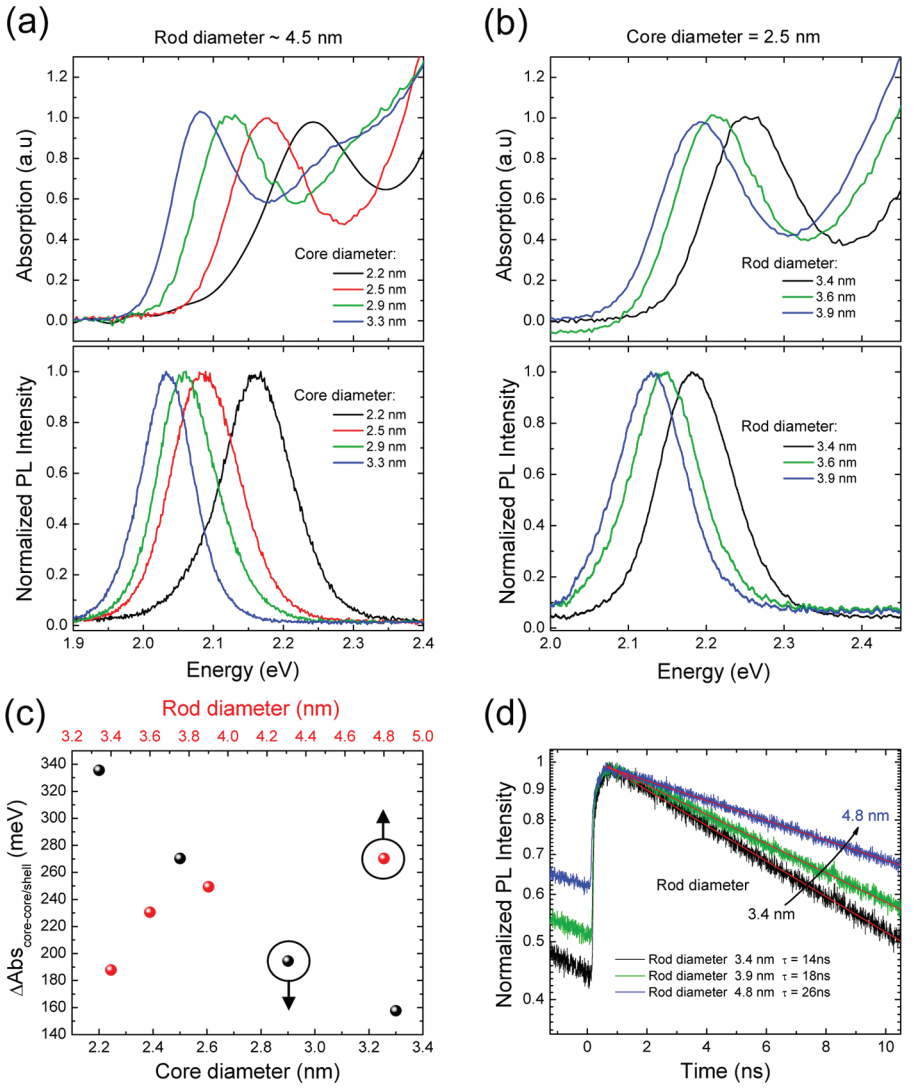

Figure 2. Basic optical properties of the samples investigated. (a) Absorption and photoluminescence spectra of a series of samples in which we independently changed the core diameter, while the rod diameter stayed approximately constant. (b) Absorption and photoluminescence spectra of a series of samples in which we changed the rod diameter, but used the same core diameter (2.5 nm). (c) Energy difference between the first exciton absorption peaks of core-only and core–shell structures as a function of the core diameter (black bullets) and the rod diameter (red bullets). (d) Time-resolved photoluminescence traces for a set of samples having a fixed core diameter (2.5 nm) and different rod diameters. A longer exciton lifetime was observed for samples with thicker rods because of the increase in the electron delocalization, which results in a reduced electron–hole spatial wave function overlap.

been observed for samples having a larger rod diameter. Both observations suggest that the (de)localization of electron–hole wave functions is dominated by the geometry of the heterostructure and can be fully controlled by changing the core and the rod diameters. Support for this interpretation comes from time-resolved photoluminescence (TRPL) experiments. Recently, we have demonstrated that the exciton lifetime strongly depends on the core diameter if the rod diameter is kept constant.[32] In particular, smaller core heterostructures exhibit a longer exciton lifetime because of a modified delocalization of the electron wave function in the shallow potential well formed by the CdSe/CdS heterostructure. The hole levels are less strongly affected and remain confined in the core region because of the higher valence-band offset and the larger hole effective mass. Room-temperature TRPL traces *vs* rod diameter are reported in Figure 2d. The observed change in exciton lifetime *vs* rod diameter can be rationalized by considering that a larger rod diameter allows the electron wave function to be more delocalized in the CdS region, resulting in an increase in the exciton lifetime because of the reduced electron–hole wave function overlap. Therefore, wave function engineering provides a new degree of freedom to tune the electron–hole exchange interaction and the fine-structure splitting, well beyond what can be obtained by quantum confinement alone.

To determine the exciton fine structure, we performed low-temperature (5 K) time and spectrally

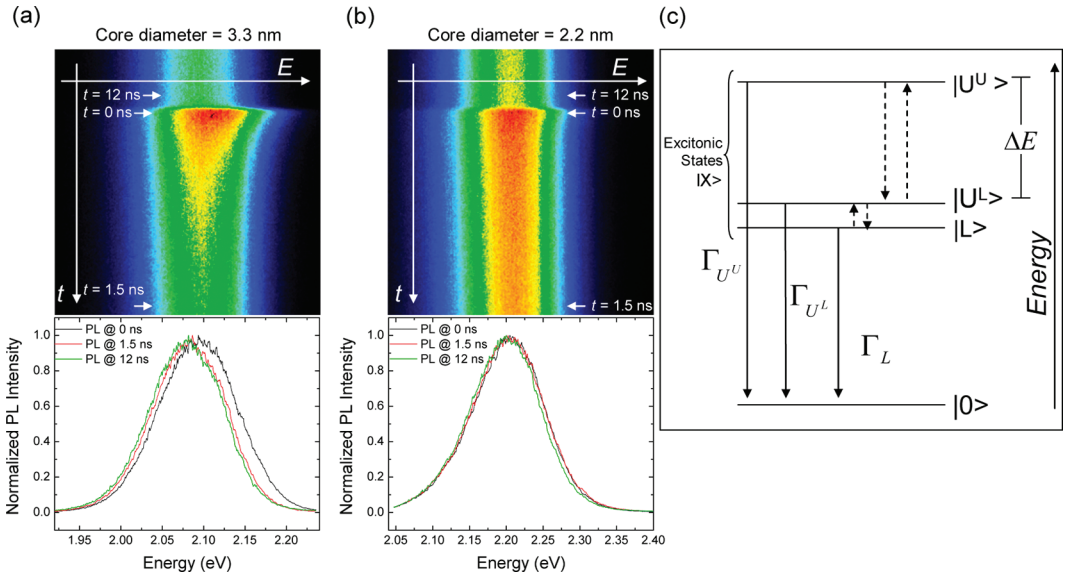

Figure 3. Unveiling the exciton fine-structure splitting by spectrally and time-resolved spectroscopy. (a) The upper panel shows the spectrally and time-resolved photoluminescence spectra obtained using a streak camera at a temperature of 5 K for a sample having a 3.3 nm core diameter. The lower panel reports the normalized PL spectra averaged over a 100 ps time window for different time delays (at 0, 1.5, and 12 ns after the pump pulse). (b) Streak image obtained for a sample with a 2.2 nm core diameter. Again, the lower panel reports the normalized PL spectra averaged over a 100 ps time window for the same different time delays as in (a). (c) Sketch of the exciton fine-structure energy levels. Three different states (U^U, U^L, and L) contribute to the low-temperature photoluminescence. The arrows indicate the intraband relaxation; $\Gamma_U{}^U$, $\Gamma_U{}^L$, and Γ_L are the radiative recombination channels.

resolved PL spectroscopy. Figure 3a reports a typical streak-camera image for samples with 3.3 nm core and 4.1 nm rod diameter. The lower part of the figure shows the PL spectra averaged over a 100 ps time window taken at different time delays (0, 1.5, and 12 ns after the pump pulse). A spectral red shift (~10 meV) of the PL maximum as a function of time is clearly observed. This behavior can be explained when considering the energy diagram of the exciton fine structure sketched in Figure 3c. We use "U" and "L" to denote the upper and lower states, respectively. We refrain from using the total angular momentum projection notation because it cannot be directly obtained from the PL measurements, and therefore the emission cannot be unambiguously assigned to specific states within the fine structure. An energetically higher lying emitting state (labeled U^U) contributes to the emission only at very early times after the pump pulse because of a fast intraband relaxation (hundred-ps time scale). For longer times, the emission is dominated by the emitting states labeled U^L and L. An energy red shift between the PL bands at 1.5 and 12 ns is also observed, which can be related to the higher contribution of the lowest emitting state L owing to its longer lifetime. As we did not observe any changes in the PL decay using different pump power and as excitation pump sources with different repetition rate also yielded similar results (see Figure S3 in the Supporting Information), we can safely exclude the contribution of multiexciton recombination to the observed behavior. Furthermore, acoustic phonons and in particular breathing modes are also ruled out given the characteristic frequency dispersion of those modes as reported in detail in the Supporting Information (Figure S4). Hence, data confirm that we are probing three different states within the exciton fine structure.

Figure 3b reports time-resolved experiments performed on a sample with 2.2 nm core and 4.7 nm rod diameter. Here, the U^U–U^L energy splitting is strongly reduced, resulting in virtually identical PL spectra at 0 and 1.5 ns. If the CdSe/CdS dot-in-rods behaved as simple CdSe core quantum dots (QDs), the opposite trend would be observed, *i.e.*, an increased energy splitting with decreasing core size (see the Supporting Information for a comparison with CdSe/ZnS QDs).[7,11] However, the 2.2 nm core size sample exhibits a longer exciton lifetime owing to the reduced electron–hole spatial overlap.

Among the various effects that contribute to the fine-structure splitting, the electron–hole exchange interaction plays an important role.[7,31] The exchange energy, in its general form, is proportional to the integral[33]

$$E \propto \int\int d^3r_1 d^3r_2 \Psi^*_X(\mathbf{r}_e = \mathbf{r}_1, \mathbf{r}_h = \mathbf{r}_2) \times \frac{1}{|\mathbf{r}_1 - \mathbf{r}_2|} \Psi_X(\mathbf{r}_e = \mathbf{r}_2, \mathbf{r}_h = \mathbf{r}_1) \quad (1)$$

where Ψ_X is the exciton wave function and $\mathbf{r}_e$ and $\mathbf{r}_h$ are the electron and hole coordinates, respectively. This

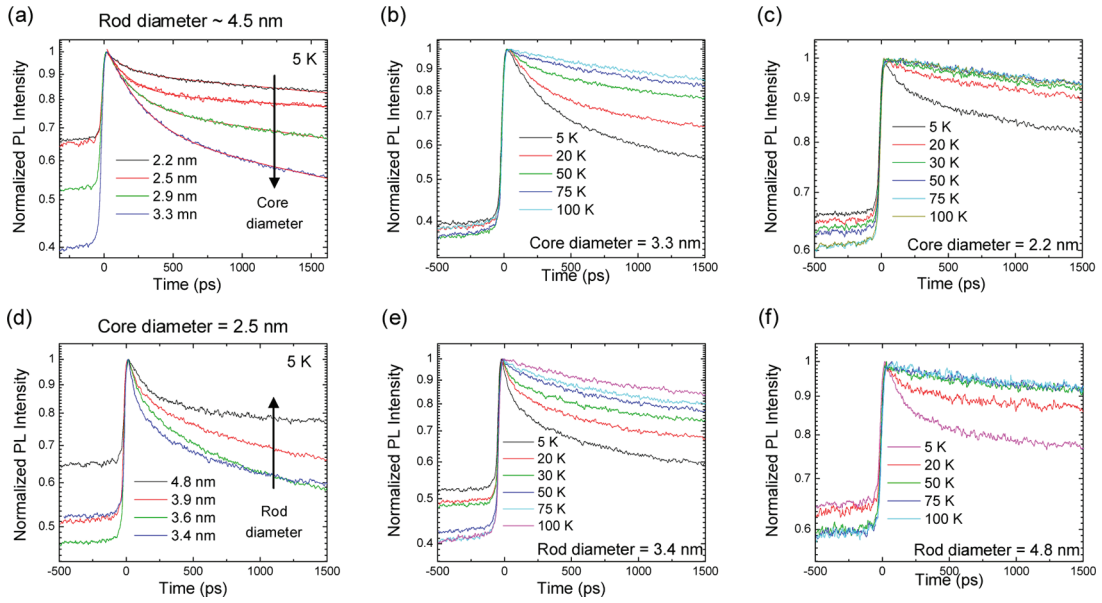

Figure 4. Revealing the exciton fine-structure splitting by temperature-dependent time-resolved spectroscopy. (a) Spectrally integrated time-resolved traces for samples having roughly the same rod diameter and different core diameters, obtained at 5 K. (b and c) Time-resolved traces as a function of the temperature for the samples with a 3.3 and a 2.2 nm core diameter, respectively. (d) Spectrally integrated time-resolved traces for samples having the same core diameter (2.5 nm) and different rod diameters, obtained at 5 K. (e and f) Time-resolved traces as a function of the temperature for the samples with a 3.4 nm and a 4.8 nm rod diameter, respectively.

integral can be divided into two parts: a short- and a long-range part. The short-range interaction is governed by an electron and a hole in the same unit cell, which splits the 8-fold exciton state into five different states, and it is the subject of this study. The long-range interaction is based on electrons and holes located in different unit cells and mainly induces a splitting of the bright exciton states. It has been experimentally demonstrated that both types of interactions are linked to the spatial electron–hole wave function overlap.[14,16,31,33] Therefore, the reduced splitting is a direct measure of the reduced electron–hole exchange interaction.

Further understanding comes from the analysis of the spectrally integrated (over the entire emission band) PL decay, as shown in Figure 4. In particular, Figure 4a shows the PL decay of samples having different core diameters and roughly the same rod diameter (~4.5 nm). The traces can be fitted well by a biexponential decay function. This yields a slow component on the order of tens of nanoseconds, which is mainly due to radiative recombination from the lower energy states, and a fast component on the order of hundreds of picoseconds. The decay time of the slow component decreases with increasing core diameter, in agreement with room-temperature results (see Figure 2),[32] confirming that the electron–hole spatial wave function overlap increases with increasing the core diameter. The fast component is related to hot-exciton relaxation within the fine structure and could be attributed to the interaction of excitons with defect states, phonon states, or vibrational states in the ligands surrounding the nanoparticles.[34,35]

Figure 4b and c report the temperature-dependent PL decay for samples with 3.3 and 2.2 nm core diameters, respectively. The results show that the fast component disappears with increasing temperature owing to thermally assisted population of the upper energy state according to a Boltzmann distribution. At high temperatures, this results in a monoexponential decay of an effective state constituted by the two states U^U and U^L in thermal equilibrium. What is remarkably different is the rate at which the thermalization occurs. In fact, a temperature as high as 70 K is needed for the sample with a 3.3 nm core, whereas for the sample with a core diameter of 2.2 nm, the decay is monoexponential already at 30 K. This again substantiates the existence of a strongly reduced fine-structure splitting for the sample with a 2.2 nm core size, as suggested by the spectrally resolved analysis.

The same behavior is observed for samples having a fixed core diameter (2.5 nm) and different rod diameters (see Figure 4d). Again in this case, the slow component is related to the radiative recombination from the lower emitting states and is in agreement with the room-temperature results: thicker rod samples show longer exciton lifetimes owing to the reduced electron–hole spatial overlap. Figure 4e and f report the temperature-dependent TRPL traces for samples with 3.4 and 4.8 nm rod diameters, respectively. The two samples exhibit distinctively different thermalization behavior because thermalization in samples with thicker rods is much faster because of the reduced fine-structure splitting.

To derive the energy splitting quantitatively, we have used a three-level model consisting of one ground state

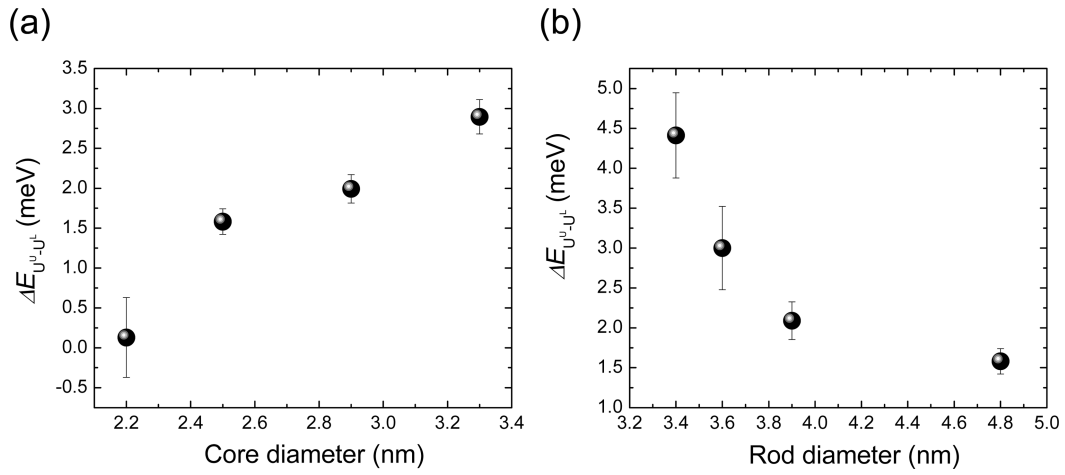

Figure 5. Control over the fine-structure splitting by precisely engineering the nano-heterojunction. The measured energy splitting *vs* core diameter (having roughly the same rod diameter of ~4.5 nm) and rod diameter (with 2.5 nm core diameter) is reported in (a) and (b), respectively.

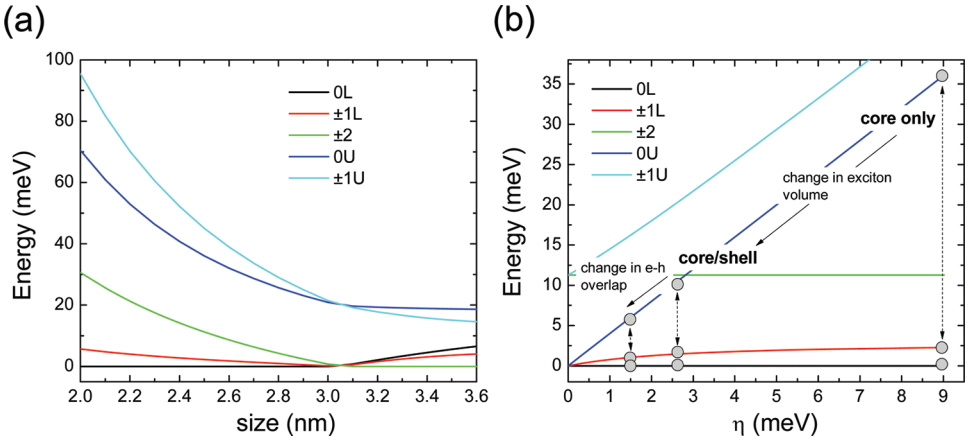

Figure 6. (a) Size dependence of the exciton band-edge fine structure considering a QD aspect ratio of 1.15 calculated in the effective mass approximation. (b) Energy splitting *vs* the parameter η. The three vertical arrows denote three different situations: core only; core/shell structure with an increased exciton volume, and core/shell with a reduced electron–hole overlap. The size of the gray dots represents the ultimate potential experimental resolution related to the thermal energy (at T = 5 K, k_BT is about 0.45 meV).

and two excited states. In doing so, we have assumed that the observed dynamics in the first 2 ns is mainly dominated by the two upper emitting states (U^U and U^L) because the decay time of the lower state is more than an order of magnitude longer. The model describes the dynamics well, and the results of the fitting are summarized in Figure 5 (see the Supporting Information for details on the fitting procedure).

Figure 5a presents the results for samples having different core diameters. As anticipated by the analysis above, the sample with a 2.2 nm core diameter exhibits a strongly reduced energy splitting. Note that the opposite behavior is expected for spherical bare CdSe QDs.[7,11] This confirms that the energy splitting is dominated by electron–hole spatial wave function overlap in addition to the physical dimension of the core. Figure 5b shows the results obtained by changing the rod diameter. Samples with a larger rod diameter exhibit reduced splitting as a result of the reduced electron–hole exchange interaction. Note that the analysis above concerning the energetic splitting between U^U and U^L states profoundly differs from what is reported in the literature,[8–10,31] where usually the splitting between L and U^L states (dark–bright splitting) is investigated.

In the following we rationalize the observed decrease in the splitting energy in the framework of the effective mass approximation. This already gives a quantitative estimate in the right order of magnitude, while full and possibly more precise quantum mechanical methods (*i.e.*, advanced semiempirical pseudopotential method) would be beyond the scope of this paper. Figure 6a reports the size-dependent fine-structure splitting based on such calculations. We have recently demonstrated that for very small particles the shape anisotropy plays an important role.[11] Taking this into account and considering that we investigated anisotropic dot-in-rod structures, we have considered

a typical QD aspect ratio of 1.15. As can be clearly observed, the splitting decreases by increasing the particles size. Following the seminal work of Efros *et al.*,[7] three effects contribute to the splitting: the crystal field, the shape anisotropy, and the electron–hole exchange interaction. The latter can be modeled as follows:

$$\eta = \left(\frac{a_{ex}}{a}\right)^3 \hbar\omega_{ST}\chi(\beta) \quad (2)$$

where a_{ex} is Bohr radius, a the physical size of the nanocrystal, $\hbar\omega_{ST}$ is the bulk splitting energy, and $\chi(\beta)$ a dimensionless function that assumes the value of 0.77 in CdSe crystals.[7]

For a comparison with the experiments, we have considered the case of a bare nanocrystal of 2.5 nm. According to eq 2, η assumes a value of 9 meV. In order to highlight the influence of the exchange interaction, we plot in Figure 6b the fine-structure energy levels as a function of η in the range 0–9 meV, where 0 meV corresponds to the limit of complete electron–hole separation. The graph allows discussing qualitatively the splitting energies induced by a change in the exchange interaction through shell deposition and electron delocalization. After shell deposition, we have observed a shift of the absorption peak (Figure 2), which can be linked to a change in exciton volume, as a result of the electron wave function delocalization in the shell region. Considering the shift in absorption (~300 meV) and the sizing curve for wurtzite CdSe nanocrystals,[36] we have estimated a change in the effective size from 2.5 to 3.8 nm. This reduces the value of η by a factor 3.5 and consequently induces a decrease in the splitting energy. The electron wave function delocalization also leads to a change in the electron–hole overlap (the hole levels are unaffected and remain confined in the core region because of the higher valence band offset and the higher hole effective mass). Comparing CdSe/ZnS[11] and CdSe/CdS nanoparticles,[32] we have measured an increase in the radiative lifetime by a factor of 2 for the latter system. This effect further reduces the value of η approximately down to 1.5 meV. Taking into account the approximations made, the splitting energy between the 0 U and ±1 L states (~4 meV) is then in reasonable agreement with the experimentally measured splitting energy (1.5 meV). A full quantum mechanical calculation might further improve agreement between experiment and theory; yet this is beyond the scope of the present study, where we aim to demonstrate that well-engineered nanojunctions provide a new degree of freedom to tune the electron–hole exchange interaction and the fine-structure splitting, well beyond what can be obtained by quantum confinement alone.

CONCLUSIONS

We have shown that a strong reduction of the energy splitting of the exciton fine structure can be achieved by changing the core and/or the rod diameter, whereby the electron–hole spatial wave function overlap can be adjusted. One can anticipate that this type of control on the short-ranged exchange interaction can be extended to the long-ranged one, which dominates the fine-structure splitting of bright excitons. The exciting tuning capabilities of colloidal quantum dots now start to extend beyond simple wavelength tuning and enable real quantum engineering of the energy levels. Therefore, understanding and controlling the fine-structure splitting has important implications in the field of optical quantum communication and could, in particular, pave the way toward a new source of entangled photon pairs.

METHODS

Sample Preparation. CdSe/CdS nanorods were synthesized according to an established procedure.[20] First, CdSe cores (seeds) are synthesized in trioctylphosphinoxide (TOPO), using a mixture of cadmium oxide (CdO) octadecylphosphonic acid, and trioctylphosphineselenide (TOPSe) as precursors. To synthesize the CdSe/CdS nanorods, the CdSe seeds are co-injected with a TOPS precursor into a hot reaction mixture containing octadecyl- and hexylphosphonic acid, TOPO and CdO.

Structural Characterization. Transmission electron microscopy measurements were carried out using a JEOL FE2200. Analysis of the nanorod length and diameter was performed using DigitalMicrograph software.

Optical Characterization. For optical measurements, thin films (micrometer range) were prepared by drop-casting QD solutions (10 μM in toluene) on a precleaned glass substrate. Time-integrated photoluminescence spectra were measured using a Hitachi F4500 fluorescence spectrometer with a xenon lamp as excitation source. Time-resolved photoluminescence spectroscopy was performed by exciting the samples with a frequency-doubled Ti:sapphire mode-locked laser delivering pulses of about 100 fs duration at 400 nm and a repetition rate of 80 MHz (additional measurements using a repetition rate of 1 kHz are reported in the Supporting Information). The photoluminescence was recorded by an avalanche photodiode in combination with a time-correlated single-photon counting module (time resolution of about 100 ps). Moreover, for spectrally and time-resolved measurements, the photoluminescence was dispersed by a grating with 150 grooves/mm in a 300 mm spectrograph and finally detected using a Hamamatsu C5680 streak camera with 2 ps time resolution.

Conflict of Interest: The authors declare no competing financial interest.

Acknowledgment. We thank B. Mazenauer and D. Caimi for their technical support and F. Ding, G. Signorello, and B. J. Offrein for stimulating discussions. The research leading to these results received funding from the European Community's Seventh Framework Programme under grant agreement no. 214954 (HERODOT). I.M. is a postdoctoral researcher with the FWO-Vlaanderen. Z.H. acknowledges BelSPo (IAP 6.10: photonics@be) and the FWO-Vlaanderen (project no. G.0794.10) for financial support.

Supporting Information Available: Additional data on the structural and optical properties of CdSe/CdS dot-in-rod structures

are reported. Details on the fitting procedure are also included. This material is available free of charge via the Internet at http://pubs.acs.org.

REFERENCES AND NOTES

1. Coe, S.; Woo, W. K.; Bawendi, M. G.; Bulovic, V. Electroluminescence from Single Monolayers of Nanocrystals in Molecular Organic Devices. *Nature* **2002**, *420*, 800–803.
2. Greenham, N. C.; Peng, X.; Alivisatos, A. P. Charge Separation and Transport in Conjugated-Polymer/Semiconductor-Nanocrystal Composites Studied by Photoluminescence Quenching and Photoconductivity. *Phys. Rev. B* **1996**, *54*, 17628–17637.
3. Klimov, V. I.; Mikhailovsky, A. A.; Xu, S.; Malko, A.; Hollingworth, J. A.; Leatherdale, C. A.; Eisler, H.-J.; Bawendi, M. G. Optical Gain and Stimulated Emission in Nanocrystal Quantum Dots. *Science* **2000**, *290*, 314.
4. Lee, J. S.; Kovalenko, M. V.; Huang, J.; Chung, D. S.; Talapin, D. V. Band-Like Transport, High Electron Mobility and High Photoconductivity in All-Inorganic Nanocrystal Arrays. *Nat. Nanotechnol.* **2011**, *6*, 348–352.
5. Pisanello, F.; Martiradonna, L.; Leménager, G.; Spinicelli, P.; Fiore, A.; Manna, L.; Hermier, J. P.; Cingolani, R.; Giacobino, E.; De Vittorio, M.; *et al.* Room Temperature-Dipolelike Single Photon Source with a Colloidal Dot-in-Rod. *Appl. Phys. Lett.* **2010**, *96*, 033101.
6. Nair, G.; Zhao, J.; Bawendi, M. G. Biexciton Quantum Yield of Single Semiconductor Nanocrystals from Photon Statistics. *Nano Lett.* **2011**, *11*, 1136–1140.
7. Efros, Al. L.; Rosen, M.; Kuno, M.; Nirmal, M.; Norris, D. J.; Bawendi, M. Band-Edge Exciton in Quantum Dots of Semiconductors with a Degenerate Valence Band: Dark and Bright Exciton States. *Phys. Rev. B* **1996**, *54*, 4843–4856.
8. Nirmal, M.; Norris, D. J.; Kuno, M.; Bawendi, M. G. Observation of the "Dark Exciton" in CdSe Quantum Dots. *Phys. Rev. Lett.* **1995**, *75*, 3728–3731.
9. Le Thomas, N.; Herz, E.; Schöps, O.; Woggon, U.; Artemyev, M. V. Exciton Fine Structure in Single CdSe Nanorods. *Phys. Rev. Lett.* **2005**, *94*, 016803.
10. Biadala, L.; Louyer, Y.; Tamarat, Ph.; Lounis, B. Direct Observation of the Two Lowest Exciton Zero-Phonon Lines in Single CdSe/ZnS Nanocrystals. *Phys. Rev. Lett.* **2009**, *103*, 037404, and references therein..
11. Moreels, I.; Rainò, G.; Gomes, R.; Hens, Z.; Stöferle, T.; Mahrt, R. F. Band-Edge Exciton Fine Structure of Small, Nearly Spherical Colloidal CdSe/ZnS Quantum Dots. *ACSNano* **2011**, *5*, 8033–8039.
12. Benson, O.; Santori, C.; Pelton, M.; Yamamoto, Y. Regulated and Entangled Photons from a Single Quantum Dot. *Phys. Rev. Lett.* **2000**, *84*, 2513.
13. Stevenson, R. M.; Young, R. J.; Atkinson, P.; Cooper, K.; Ritchie, D. A.; Shields, A. J. A Semiconductor Source of Triggered Entangled Photon Pairs. *Nature* **2006**, *439*, 179–182.
14. Seguin, R.; Schliwa, A.; Germann, T. D.; Rodt, S.; Pötschke, K.; Strittmatter, A.; Pohl, U. W.; Bimberg, D.; Winkelnkemper, M.; Hammerschmidt, T.; *et al.* Control of Fine-Structure Splitting and Excitonic Binding Energies in Selected Individual InAs/GaAs Quantum Dots. *Appl. Phys. Lett.* **2006**, *89*, 263109.
15. Singh, R.; Bester, G. Nanowire Quantum Dots as an Ideal Source of Entangled Photon Pairs. *Phys. Rev. Lett.* **2009**, *103*, 063601.
16. Bennett, A. J.; Pooley, M. A.; Stevenson, R. M.; Ward, M. B.; Patel, R. B.; Boyer de la Giroday, A.; Sköld, N.; Farrer, I.; Nicoll, C. A.; Ritchie, D. A.; *et al.* Electric-Field-Induced Coherent Coupling of the Exciton States in a Single Quantum Dot. *Nat. Phys.* **2010**, *6*, 947–950.
17. He, J.; Lo, S. S.; Kim, J.; Scholes, G. D. Control of Exciton Spin Relaxation by Electron–Hole Decoupling in Type-II Nanocrystal Heterostructures. *Nano Lett.* **2008**, *8*, 4007–4013.
18. Kim, J.; Wong, C. Z.; Scholes, G. D. Exciton Fine Structure and Spin Relaxation in Semiconductor Colloidal Quantum Dots. *Acc. Chem. Res.* **2009**, *4*, 1375–1384.
19. Talapin, D. V.; Koeppe, R.; Götzinger, S.; Kornowski, A.; Lupton, J. M.; Rogaci, A. L.; Benson, O.; Feldmann, J.; Weller, H. Highly Emissive Colloidal CdSe/CdS Heterostrucutres of Mixed Dimensionality. *Nano Lett.* **2003**, *3*, 1677–1681.
20. Carbone, L.; Nobile, C.; De Giorgi, M.; Della Sala, F.; Morello, G.; Pompa, P.; Hytch, M.; Snoeck, E.; Fiore, A.; Franchini, I. R.; *et al.* Synthesis and Micrometer-scale Assembly of Colloidal CdSe/CdS Nanorods Prepared by a Seeded Growth Approach. *Nano Lett.* **2007**, *7*, 2942–2950.
21. Talapin, D. V.; Nelson, J. H.; Shevchenko, E. V.; Aloni, S.; Sadtler, B.; Alivisatos, A. P. Seeded Growth of Highly Luminescent CdSe/CdS Nanoheterostructures with Rod and Tetrapod Morphologies. *Nano Lett.* **2007**, *7*, 2951–2959.
22. Borys, N. J.; Walter, M. J.; Huang, J.; Talapin, D. T.; Lupton, J. M. The Role of Particle Morphology in Interfacial Energy Transfer in CdSe/CdS Heterostructure Nanocrystals. *Science* **2010**, *330*, 1371.
23. Sitt, A.; Della Sala, F.; Menagen, G.; Banin, U. Multiexciton Engineering in Seeded Core/Shell Nanorods: Transfer from Type-I to Quasi-type-II Regimes. *Nano Lett.* **2009**, *9*, 3470–3476.
24. Müller, J.; Lupton, J. M.; Lagoudakis, P. G.; Schindler, F.; Koeppe, R.; Rogach, A. L.; Feldmann, J.; Talapin, D. V.; Weller, H. Wave Function Engineering in Elongated Semiconductor Nanocrystals with Heterogeneous Carrier Confinement. *Nano Lett.* **2005**, *5*, 2044–2049.
25. Mahler, B.; Spinicelli, P.; Buil, S.; Quelin, X.; Hermier, J.-P.; Dubertret, B. Towards Non-Blinking Colloidal Quantum Dots. *Nat. Mater.* **2008**, *7*, 659–664.
26. Chen, Y.; Vela, J.; Htoon, H.; Casson, J. L.; Werder, D. J.; Bussian, D. A.; Klimov, V. I.; Hollingsworth, J. A. "Giant" Multishell CdSe Nanocrystal Quantum Dot with Suppressed Blinking. *J. Am. Chem. Soc.* **2008**, *130*, 5026–5027.
27. Htoon, H.; Malko, A. V.; Bussian, D.; Vela, J.; Chen, Y.; Hollingsworth, J. A.; Klimov, V. I. Highly Emissive Multiexcitons in Steady-State Photoluminescence of Individual "Giant" CdSe/CdS Core/Shell Nanocrystals. *Nano Lett.* **2010**, *10*, 2401–2407.
28. García-Santamaría, F.; Chen, Y.; Vela, J.; Schaller, R. D.; Hollingsworth, J. A.; Klimov, V. I. Suppressed Auger Recombination in "Giant" Nanocrystals Boosts Optical Gain Performance. *Nano Lett.* **2009**, *9*, 3482–3488.
29. Zavelani-Rossi, M.; Lupo, M. G.; Tassone, F.; Manna, L.; Lanzani, G. Suppression of Biexciton Auger Recombination in CdSe/CdS Dot/Rods: Role of the Electronic Structure in the Carrier Dynamics. *Nano Lett.* **2010**, *10*, 3142–3150.
30. García-Santamaría, F.; Brovelli., S.; Viswanatha, R.; Hollingsworth, J. A.; Htoon, H.; Crooker, S. A.; Klimov, V. I. Breakdown of Volume Scaling in Auger Recombination in CdSe/CdS Heteronanocrystals: The Role of the Core–Shell Interface. *Nano Lett.* **2011**, *11*, 687–693.
31. Brovelli. S.; Schaller, R. D.; Crooker, S. A.; García-Santamaría, F.; Chen, Y.; Viswanatha, R.; Hollingsworth, J. A.; Htoon, H.; Klimov, V. I. Nano-engineered Electron–Hole Exchange Interaction Controls Exciton Dynamics in Core–Shell Semiconductor Nanocrystals. *Nat. Commun.* **2011**, *2*, 280, doi: 10.1038/ncomms1281.
32. Rainò, G.; Stöferle, T.; Moreels, I.; Gomes, R.; Kamal, J. S.; Hens, Z.; Mahrt, R. F. Probing the Wave Function Delocalization in CdSe/CdS Dot-in-Rod Nanocrystals by Time- and Temperature-Resolved Spectroscopy. *ACSNano* **2011**, *5*, 4031–4036.
33. Bayer, M.; Ortner, G.; Stern, O.; Kuther, A.; Gorbunov, A. A.; Forchel, A.; Hawrylak, P.; Fafard, S.; Hinzer, K.; Reinecke, T. L.; *et al.* Fine Structure of Neutral and Charged Excitons in Self-Assembled In(Ga)As/(Al)GaAs Quantum Dots. *Phys. Rev. B* **2002**, *65*, 195315.

34. Pandey, A.; Guyot-Sionnest, P. Slow Electron Cooling in Colloidal Quantum Dots. *Science* **2008**, *322*, 929.
35. Allan, G.; Delerue, C. Fast relaxation of Hot Carriers by Impact Ionization in Semiconductor Nanocrystals: Role of Defects. *Phys. Rev. B* **2009**, *79*, 195324.
36. Jasieniak, J.; Smith, L.; van Embden, J.; Mulvanez, P.; Califano, M. Re-Examination of the Size-Dependent Absorption Properties of CdSe Quantum Dots. *J. Phys. Chem. C* **2009**, *113*, 19468.